# Coherent Optical Spectroscopy of a Strongly Driven Quantum Dot

Xiaodong Xu, *et al.*

*Science* **317**, 929 (2007);
DOI: 10.1126/science.1142979

field of the form $M(y)P_\ell(y)$ can be obtained by introducing a slowly varying modulation in, say, the width or the properties of the material of which an element is made. Similarly, in the case of azimuthal symmetry, a Bessel beam can be used together with a set of concentric rings of properly modulated width placed at radii satisfying $J_1(q_0\rho) = 0$. The technology for manufacturing plates of this kind for microwave applications has been available for quite some time, whereas nanofabrication methods involving, for example, electron and focused ion beam lithography, can be used for the infrared and optical range. An important consideration in the design of a near-field plate is to avoid as much as possible the presence of terms giving a background that could overwhelm the sharp features of the field. An example of background-free focusing is shown in Fig. 2. These results are for the diffraction of a plane wave by a set of ribbons of very narrow width $<< \ell$ and parameters such that the total current density is $\mathbf{j} = (j_x,0,0)$ where

$$j_x \propto \delta(z) \sum_{s=-\infty}^{\infty} \frac{(-1)^s \delta(y - s\ell)}{(1 + s^2\ell^2/L^2)} \qquad (7)$$

(the incident electric field is parallel to the cylindrical axis). Such an array of currents, with the sign varying from one element to the next, can be realized at infrared and optical frequencies by alternating material with positive and negative permittivity and, in the microwave regime, by using a set of interchanging capacitive and inductive elements. Figure 2B shows a contour plot of the $y$ component of the diffracted magnetic field (logarithmic scale). These results are similar to those reported for negative-index slabs (*14*, *25*), thereby revealing the close relationship between the two phenomena (*26*). Finally, to help ascertain the origin of radiationless interference, we show in Fig. 2C a linear plot of the field intensity, normalized to its largest value at a given $z$. Reflecting a property of the zeros of $H_y$, the figure clearly shows behavior reminiscent of beam coupling in that the diffraction of the beam produced by a particular current source is prevented by the presence of its neighbors. It is only after the intensity of its neighbors has decreased a sufficient amount that the central beam is allowed to spread, and the point at which this happens determines the focal length.


**References and Notes**

1. E. Abbe, *Arch. Mikrosk. Anat.* **9**, 413 (1873).
2. E. Betzig, J. K. Trautman, *Science* **257**, 189 (1992).
3. A. Tselev *et al.*, *Rev. Sci. Instrum.* **74**, 3167 (2003).
4. F. Zenhausern, Y. Martin, H. K. Wickramasinghe, *Science* **269**, 1083 (1995).
5. R. Hillenbrand, T. Taubner, F. Keilmann, *Nature* **418**, 159 (2002).
6. M. I. Stockman, S. V. Faleev, D. J. Bergman, *Phys. Rev. Lett.* **88**, 067402 (2002).
7. G. Lerosey, J. de Rosny, A. Tourin, M. Fink, *Science* **315**, 1120 (2007).
8. P. C. M. Planken, N. C. J. van der Valk, *Opt. Lett.* **29**, 2306 (2004).
9. D. R. Smith, J. B. Pendry, M. C. K. Wiltshire, *Science* **305**, 788 (2004).
10. D. R. Smith, *Science* **308**, 502 (2005).
11. J. B. Pendry, *Phys. Rev. Lett.* **85**, 3966 (2000).
12. N. A. P. Nicorovici, R. C. McPhedran, G. W. Milton, *Phys. Rev. B* **49**, 8479 (1994).
13. G. W. Milton, N. A. P. Nicorovici, R. C. McPhedran, V. A. Podolskiy, *Proc. R. Soc. London Ser. A* **461**, 3999 (2005).
14. R. Merlin, *Appl. Phys. Lett.* **84**, 1290 (2004).
15. R. Shelby, D. R. Smith, S. Schultz, *Science* **292**, 77 (2001).
16. A. Grbic, G. V. Eleftheriades, *Phys. Rev. Lett.* **92**, 117403 (2004).
17. N. Fang, H. Lee, C. Sun, X. Zhang, *Science* **308**, 534 (2005).
18. T. Taubner, D. Korobkin, Y. Urzhumov, G. Shvets, R. Hillenbrandt, *Science* **313**, 1595 (2006).
19. E. Hecht, *Optics* (Addison Wesley, San Francisco, 2002).
20. J. A. Stratton, *Electromagnetic Theory* (McGraw-Hill, New York, 1941).
21. P. C. Clemmow, *The Plane Wave Spectrum Representation of Electromagnetic Fields* (Pergamon, Oxford, 1966).
22. J. H. McLeod, *J. Opt. Soc. Am.* **44**, 592 (1954).
23. J. Durnin, J. J. Miceli Jr., J. H. Eberly, *Phys. Rev. Lett.* **58**, 1499 (1987).
24. D. R. Smith *et al.*, *Appl. Phys. Lett.* **82**, 1506 (2003).
25. G. Shvets, *Phys. Rev. B* **67**, 035109 (2003).
26. We emphasize that, although our plates and negative-index slabs create comparable field distributions, the physical origins are very different in that the plates transform, propagating into evanescent modes, whereas the slabs amplify the near field.


27. The author acknowledges discussions with A. Grbic. This work was supported by the Air Force Office of Scientific Research under contract FA 9550-06-01-0279 through the Multidisciplinary University Research Initiative Program.

16 April 2007; accepted 27 June 2007
Published online 12 July 2007;
10.1126/science.1143884
Include this information when citing this paper.




# Coherent Optical Spectroscopy of a Strongly Driven Quantum Dot


**Xiaodong Xu,[1] Bo Sun,[1] Paul R. Berman,[1] Duncan G. Steel,[1]* Allan S. Bracker,[2] Dan Gammon,[2] L. J. Sham[3]**



**Quantum dots are typically formed from large groupings of atoms and thus may be expected to have appreciable many-body behavior under intense optical excitation. Nonetheless, they are known to exhibit discrete energy levels due to quantum confinement effects. We show that, like single-atom or single-molecule two- and three-level quantum systems, single semiconductor quantum dots can also exhibit interference phenomena when driven simultaneously by two optical fields. Probe absorption spectra are obtained that exhibit Autler-Townes splitting when the optical fields drive coupled transitions and complex Mollow-related structure, including gain without population inversion, when they drive the same transition. Our results open the way for the demonstration of numerous quantum level–based applications, such as quantum dot lasers, optical modulators, and quantum logic devices.**


The quantum optoelectronic properties of semiconductor quantum dots (QDs) have featured prominently in numerous proposals, including quantum computing, single-photon sources, and quantum repeaters (*1*–*3*). QDs are particularly attractive for these applications because they behave in many ways as simple stationary atomic or molecular systems (*4*) with discrete states where the electron-hole pair can be treated as a well-defined composite-particle state (*5*).

Whereas strong optical excitation of a semiconductor creates a many-body problem because of the extended nature of the wave function (*6*), confinement of the wave function in QDs leads to strong energy-level shifts between one exciton and two or more exciton states, enabling the system to be considered as a relatively simple few-level problem. The strong-field excitation regime of the transition from the ground state to an excited state such as the exciton, a Coulomb bound electron-hole pair, is then defined by $\Omega_R >> 2\gamma$ where the Rabi frequency $\Omega_R = \frac{\mu E}{h}$, $\gamma$ is a transition linewidth (full width at half-maximum, in Hz), $\mu$ is the transition dipole moment, and $E$ is the amplitude of the optical electric field. For time scales less than $\gamma^{-1}$, strong excitation leads to Rabi oscillations (*7*–*10*) in time. The effect of vacuum Rabi splitting (*11*) has also been observed in a single QD embedded in a nanocavity (*12*–*14*).

Under strong continuous wave (CW) narrowband resonant optical excitation of a simple atomic system, the fluorescence emission spectrum, which is a narrow emission line at low power (the emission width is the laser bandwidth), consists of three peaks referred to as the Mollow triplet (*15*). A simple picture of the origin of this emission pattern is understood from a dressed-atom picture (*16*). Figure 1B shows the dressed-state picture with fully quantized atom-field states, when the driving-field frequency $\omega$ is equal to the electronic frequency $\omega_0$. In this limit,


[1]The H. M. Randall Laboratory of Physics, The University of Michigan, Ann Arbor, MI 48109, USA. [2]The Naval Research Laboratory, Washington, DC 20375, USA. [3]Department of Physics, University of California–San Diego, La Jolla, CA 92093, USA.

*To whom correspondence should be addressed. E-mail: dst@umich.edu

the "bare" states $|3, N-1\rangle$ and $|2, N\rangle$ are degenerate, where $N$ labels the photon number of the driving field. The atom-field interaction lifts this degeneracy and produces "dressed" states $|\alpha(N-1)\rangle$ and $|\beta(N-1)\rangle$ having energy separation $\hbar\Omega_R$ as shown. The dressed states are linear combinations of the bare states. The dashed lines in the figure indicate a triplet of possible emission frequencies, occurring at $\omega$ and $\omega \pm \Omega_R$.

In absorption, the spectrum can be more complex. For the three-level V system (Fig. 1A), where the strong field couples levels 2 and 3, theory predicts that the probe absorption from level 2 to level 1 is strongly modified from the usual simple Lorentzian seen in the absence of strong-field excitation. The probe absorption splits into two resonances, known as the Autler-Townes (AT) splitting (*17*). When the probe absorption on the strongly driven transition (between levels 2 and 3) is measured, the spectrum is much richer. New physics beyond that seen in the Mollow fluorescence triplet is observed (*18*–*22*) and arises from the coherent coupling between the two optical fields. When the Rabi frequency of the strong pump field is sufficiently large, the absorption spectrum shows gain without population inversion.

We present experimental results of the AT splitting and complex Mollow absorption spectrum (MAS) using a single semiconductor QD. We coherently control the probe absorption with a strong optical field, thus demonstrating that the single QD coupled with the strong pump can function as a modulator of the probe absorption (*23*). In addition, the spectrum as a function of the probe frequency shows Rabi splitting and gain without population inversion. The results are in good agreement with the standard theory based on the optical Bloch equations. Our work demonstrates that on long time scales, the discrete energy-level spectrum of the dot is maintained even at the high field strengths needed for quantum logic operations (e.g., qubit rotations) and single-photon devices, and that the system behaves in a manner similar to that of a trapped atom. The results suggest that it should be possible to demonstrate numerous quantum level–based applications, such as dressed-state lasers (*24*), QD optical modulators (*23*), and quantum logic devices (*4*).

The system of interest is a single, neutral InAs self-assembled QD embedded in a Schottky diode structure at 5K (*25*). The typical single-beam, linear absorption spectrum of a single QD (Fig. 1C), taken with a CW laser with a 300-KHz linewidth, shows that the neutral exciton has two linearly polarized quantum transitions with orthogonal polarizations. The fine-structure splitting of the exciton states, due to the QD in-plane anisotropy (*26*), is about 15 μeV. In the corresponding energy-level diagram of the states (Fig. 1A), states $|1\rangle$ and $|3\rangle$ represent the exciton states, state $|2\rangle$ is the crystal ground state, and the two linearly polarized transitions are labeled V and H.

To analytically describe our experiments, we follow the approach used in (*17*, *19*), describing the system with the optical Bloch equations $i\hbar\frac{d\rho}{dt} = [H, \rho] + \text{Decay}$ (*27*, *28*), where $\rho$ and $H$ are the density matrix and Hamiltonian of the light-coupled QD system, respectively. The Hamiltonian is given by $H = H_0 - \vec{\mu} \cdot \vec{E}$ where $\vec{E} = \vec{E}_0 + \vec{E}_1$. $\vec{E}_0$ is the strong pump field and $\vec{E}_1$ is the weak probe field. For calculations of the absorption spectrum, we can use the semiclassical approach where the fields are taken to be classical. $H_0$ is the diagonalized Hamiltonian for the QD structure (Fig. 1A). The results of calculations in the limits appropriate to this work are provided in the Supporting Online Material (*25*). The theory is fit to experimental data with

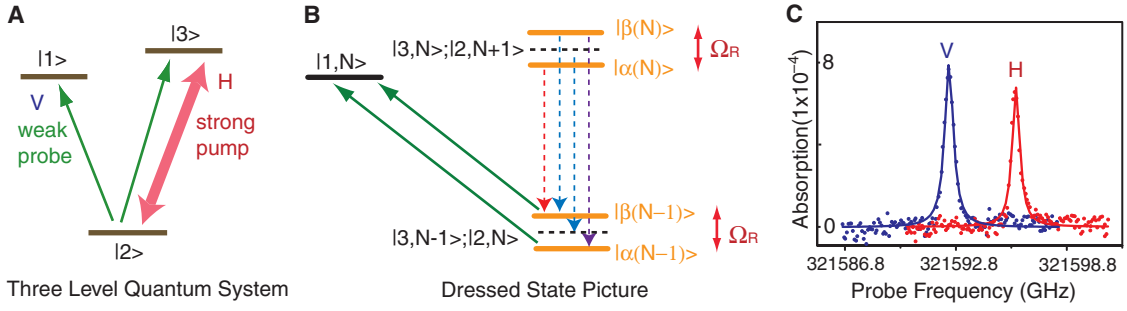


**Fig. 1.** (**A**) The energy-level diagram of a single neutral QD. The absorption of the weak probe beam by scanning either transition V or H is modified by the strong pump beam, which is near resonant with transition H. (**B**) The dressed-state picture of the system shown in (**A**). The transitions between states $|\alpha,N\rangle$ ($|\beta,N\rangle$) and $|1,N+1\rangle$, outside the energy range of the diagram, are not shown. If a weak beam probes transition 2-1 as shown by the green arrows, the absorption spectrum consists of a doublet. Ignoring the state $|1\rangle$, the emission spectrum of transition 3-2 consists of three peaks (Mollow triplet): a peak centered at the electronic transition $\omega$, and two Rabi side bands located at $\omega \pm \Omega_R$ (shown by the dashed lines). (**C**) Single-beam, linear absorption profile of a single exciton state. The horizontally (or vertically) polarized light only excites the corresponding linearly polarized exciton transition.

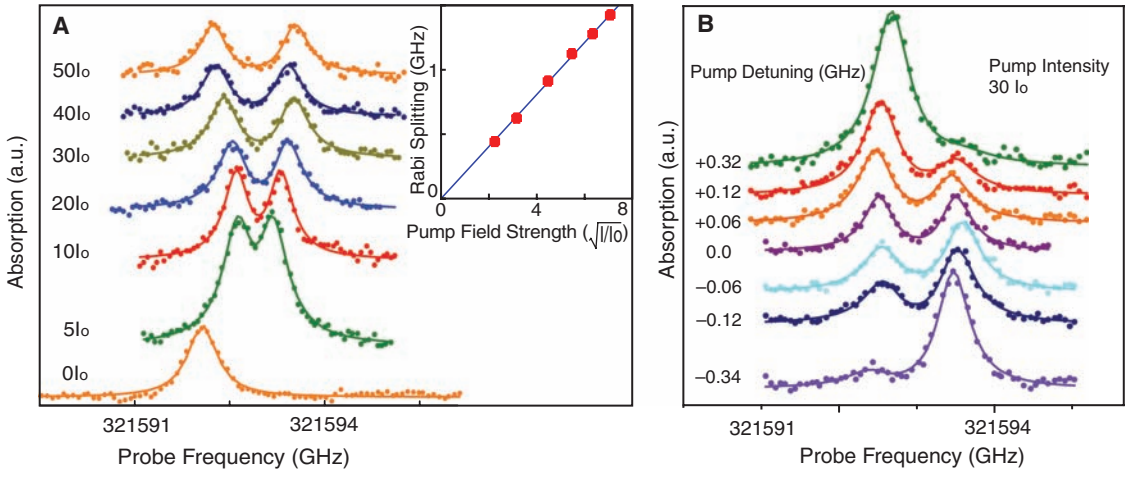


**Fig. 2.** Autler-Townes splitting by means of a single QD. A strong pump drives transition H, and a weak probe scans across transition V. (**A**) Probe absorption spectra as a function of the pump intensity when the pump is on resonance. $I_0$ equals 1.2 W/cm$^2$. The solid lines are theoretical fits to the data. The inset shows the AT splitting (Rabi splitting) as a function of the square root of the pump intensity. A linear fit (solid line) matches the data very well. (**B**) The probe absorption spectra as a function of the pump frequency detuning with fixed pump intensity. The lines are the theoretical fits to the data.

only the linewidth and amplitude as free parameters. The dipole moment is extracted from the linear dependence of the splitting on the field strength.

To experimentally demonstrate the AT effect (*17*), we use two frequency-locked but independently tunable CW lasers with a mutual coherence bandwidth of a few MHz (*25*). We set a horizontally polarized pump beam resonant with the H transition. A weak, vertically polarized probe beam then scans across transition V. The probe absorption spectra for different pump laser intensities are plotted in Fig. 2A with increasing pump intensity. The data are shifted vertically for clarity. In agreement with theory (solid lines) (*25*), the probe absorption splits into a doublet where each peak has equal strength. There is a small energy shift of the response relative to the low-intensity excitation that is probably due to a small screening of the applied field by photoexcited charge in the diode. The shift saturates at a power between the lowest-intensity curve and the next higher-power spectrum. The pump laser is adjusted to follow the shift of the resonance.

The frequency separation between the absorption peaks shows a strong dependence on the pump intensity. We plot the measured splitting as a function of the square root of the pump intensity in the inset of Fig. 2A. The splitting clearly depends linearly on the pump field strength and goes to zero in the absence of the pump, as expected for the dependence of the AT splitting on the Rabi frequency.

Figure 2B shows the probe absorption as a function of the pump detuning with a fixed pump intensity of $30I_0$ (the corresponding photon number per unit volume is ~$1.4 \times 10^{10}/\text{cm}^3$), where $I_0 = 1.2$ W/cm$^2$, corresponding to a Rabi frequency of $\sim \frac{\Omega_R}{2\pi} = 1.1$ GHz. Again, the data are shifted for clarity, and the solid lines are the fit of the data to the theory (*25*) and show good agreement.

In the MAS, where the pump and probe beams coherently couple to the same transition and the pump field is tuned to resonance, we observe a relatively weak maximum centered at zero probe detuning and two Rabi side bands with dispersive line shapes. The pump power dependence of the probe absorption spectra is shown in Fig. 3A. The single-beam absorption data are plotted at the bottom. The spectral shift of the data with the high-power optical field is due to the excitation of the charge states in the buffer layer. The complex line shape of the MAS depends strongly on the pump intensity. The splitting between the two side bands is plotted as a function of the square root of the pump intensity in Fig. 3B, again showing that the splitting linearly depends on the pump field strength and is zero in the absence of the pump field.

The data confirm that the probe beam experiences optical gain in the pump-probe configuration for strong excitation. The MAS data in Fig. 3A show that part of the probe absorption curve is below zero, which is the "gain" effect. Using the data corresponding to $15I_0$ as an example, the absorption/gain ratio is about 0.066%/0.0024% = 27.5. This gain is from the pump and probe beams coherently exchanging energy through the QD and corresponds to gain without inversion because there is no population inversion either in the dressed- or bare-atom pictures.

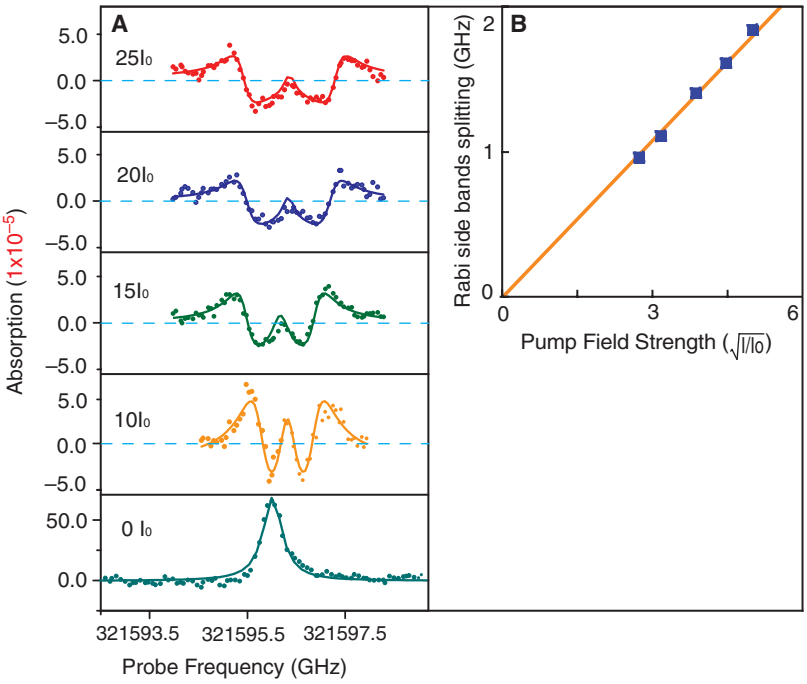


**Fig. 3.** Mollow absorption spectrum when the strong pump and weak probe beams couple to the same transition. (**A**) Measured probe absorption versus pump field intensity when the pump is on resonance. The lines are the fits to the probe absorption function obtained by solving optical Bloch equations. The MAS data show that the part of the absorption signal is "negative." Using the data corresponding to $15I_0$ as an example, the absorption/gain ratio is about 0.066%/0.0024% = 27.5. (**B**) The splitting between the Rabi side bands versus pump field strength. The solid line is the linear fit to the data.

The AT splitting can provide a method to measure the dipole moment, as the Rabi frequency is a product of the transition dipole moment with the optical field. From the extracted Rabi splitting with the corresponding optical field strength, we can infer a transition dipole moment of about 30 D for this particular QD. The Einstein A coefficient (spontaneous emission rate) of a QD in a medium is given as $\gamma_{sp} = \frac{9n^5}{(2n^2 + n_{QD}^2)^2} \times \frac{\omega_0^3 \mu^2}{3\pi\varepsilon_0 \hbar c^3} = \frac{9n^5}{(2n^2 + n_{QD}^2)^2} \gamma_{spo}$, where $n$ ($n_{QD}$) is the refractive index of the medium (QD) and $\gamma_{spo}$ is the spontaneous emission rate of a two-level quantum system in the vacuum (*29*). By taking $n = n_{QD} = 3.44$ and inserting the experimental parameters and the extracted dipole moment into the equation, we obtain $\frac{\gamma_{sp}}{2\pi} = 190$ MHz, which corresponds to a life time of about 840 ps. Assuming there is no other decay and no pure dephasing, this would lead to a natural linewidth expected in the low-power absorption spectrum also equal to $\frac{\gamma_3}{2\pi} = 190$ MHz, where $\gamma_j$ is the decay rate of level $j$ in Fig. 1A. Compared to the extracted linewidth from the single-beam, low-power absorption data, which is about 500 MHz, $\gamma_{sp}$ is smaller by a factor of about 2.5. This discrepancy indicates that there is possibly a spectral wandering process that broadens the transition linewidth (*30*). This interpretation agrees with our previous study on a single charged QD, which also suggested the absence of pure dephasing.

We can also extract the exciton decay and dephasing rates from the AT splitting and MAS data. The solid lines in Fig. 2A are the theoretical fit of the AT splitting data assuming that $\gamma_3 = \gamma_1$ and $\Gamma_{13} = 0$, where $\gamma_{ij} = (\gamma_i + \gamma_j)/2 + \Gamma_{ij}$, $\gamma_{ij}$ is the total dephasing rate, and $\Gamma_{ij}$ is the contribution to the dephasing rate of the $ij$ transition from sources other than spontaneous emission. From the fits, we find $\frac{\gamma_{23}}{2\pi}$ and $\frac{\gamma_3}{2\pi}$ of (176 ± 16) MHz and (357 ± 16) MHz, respectively. The theory fits the data very well and indicates that under these experimental conditions, the single QD behaves like a single atomic system. We also fit the MAS data to theory (*25*) (solid lines in Fig. 3A). The fitting yields $\frac{\gamma_{23}}{2\pi}$ and $\frac{\gamma_3}{2\pi}$ of (230 ± 12) MHz and (315 ± 45) MHz, respectively. The value of $\frac{\gamma_{23}}{2\pi}$ is within 10% of that extracted from the low-pump field profile. The physical parameters from the MAS and AT splitting data show that the decay rate is almost twice the dephasing rate, indicating no appreciable pure dephasing. We speculate that the reason for the discrepancy between the Einstein A coefficient determined from the dipole moment (above) and the fitting parameters is again due to spectral wandering, which leads to a fit of the theory that over-

estimates the population relaxation rate. However, this remains under investigation.

The AT splitting and gain without inversion in the Mollow absorption spectrum imply that the absorption and gain inside a single QD are tunable. In the AT configuration, the absorption of the probe beam can be switched on and off by applying a strong optical field. In contrast, in the MAS experiment, the absorption of the frequency fixed probe beam can be tuned to be positive or negative (gain) by adjusting the pump field strength. Our results are the first step toward the realization of electromagnetically induced transparency and lasing without inversion in the spin-based lambda system and suggest that QDs offer the potential to be used as elements in optoelectronics and quantum logic devices (*4*, *27*).

*Note added in proof*: Since the submission of this paper, two papers have appeared on http://arxiv.org that report studies of the resonant excitation of quantum dots in the strong excitation regime. The first (*31*) reports a measurement of the fluorescence correlation function that Mollow first calculated, and the second (*32*) reports Rabi oscillations.


**References and Notes**

1. D. Loss, D. P. DiVincenzo, *Phys. Rev. A.* **57**, 120 (1998).
2. Z. Yuan *et al.*, *Science* **295**, 102 (2002).
3. H.-J. Briegel, W. Duer, J. I. Cirac, P. Zoller, *Phys. Rev. Lett.* **81**, 5932 (1998).
4. D. Gammon, D. G. Steel, *Phys. Today* **55**, 36 (2002).
5. L. J. Sham, T. M. Rice, *Phys. Rev.* **144**, 708 (1966).
6. V. M. Axt, A. Stahl, *Z. Phys. B* **93**, 195 (1994).
7. T. H. Stievater *et al.*, *Phys. Rev. Lett.* **87**, 133603 (2001).
8. H. Kamada, H. Gotoh, J. Temmyo, T. Takagahara, H. Ando, *Phys. Rev. Lett.* **87**, 246401 (2001).
9. H. Htoon *et al.*, *Phys. Rev. Lett.* **88**, 087401 (2002).
10. A. Zrenner *et al.*, *Nature* **418**, 612 (2002).
11. J. J. Sanchez-Mondragon, N. B. Narozhny, J. H. Eberly, *Phys. Rev. Lett.* **51**, 550 (1983).
12. J. P. Reithmaier *et al.*, *Nature* **432**, 197 (2004).
13. T. Yoshie *et al.*, *Nature* **432**, 200 (2004).
14. K. Hennessy *et al.*, *Nature* **445**, 896 (2007).
15. B. R. Mollow, *Phys. Rev.* **188**, 1969 (1969).
16. J. Dupont-Roc, G. Grynberg, C. Cohen-Tannoudji, *Atom-Photon Interactions: Basic Processes and Applications* (Wiley, New York, 1998).
17. S. H. Autler, C. H. Townes, *Phys. Rev.* **100**, 703 (1955).
18. E. V. Baklanov, V. P. Chebotaev, *Sov. Phys. JETP* **34**, 490 (1972).
19. B. R. Mollow, *Phys. Rev. A.* **5**, 2217 (1972).
20. S. Haroche, F. Hartmann, *Phys. Rev. A.* **6**, 1280 (1972).
21. F. Y. Wu, S. Ezekiel, M. Ducloy, B. R. Mollow, *Phys. Rev. Lett.* **38**, 1077 (1977).
22. M. T. Gruneisen, K. R. MacDonald, R. W. Boyd, *J. Opt. Soc. Am. B* **5**, 123 (1988).
23. S. G. Carter *et al.*, *Science* **310**, 651 (2005).
24. N. Lu, P. R. Berman, *Phys. Rev. A.* **44**, 5965 (1991).
25. Materials and methods are available as supporting material on *Science* Online.
26. D. Gammon, E. S. Snow, B. V. Shanabrook, D. S. Katzer, D. Park, *Phys. Rev. Lett.* **76**, 3005 (1996).
27. M. O. Scully, M. S. Zubairy, *Quantum Optics* (Cambridge Univ. Press, Cambridge, 1997).
28. P. Meystre, M. Sargent, *Elements of Quantum Optics* (Springer-Verlag, Heidelberg, Germany, ed. 3, 1998) chap. 9.
29. A. Thranhardt, C. Ell, G. Khitrova, H. M. Gibbs, *Phys. Rev. B* **65**, 035327 (2002).
30. A. Hogele *et al.*, *Phys. Rev. Lett.* **93**, 217401 (2004).
31. A. Muller *et al.*, http://arxiv.org/abs/0707.0656.
32. R. Melet *et al.*, http://arxiv.org/abs/0707.3061.



33. This work is supported by the U.S. Army Research Office, Air Force Office of Scientific Research, Office of Naval Research, NSA/LPS, and FOCUS-NSF.


**Supporting Online Material**

www.sciencemag.org/cgi/content/full/317/5840/929/DC1
Materials and Methods
SOM Text
Fig. S1
References


26 March 2007; accepted 4 June 2007
10.1126/science.1142979


# Deep Ultraviolet Light–Emitting Hexagonal Boron Nitride Synthesized at Atmospheric Pressure


**Yoichi Kubota,* Kenji Watanabe, Osamu Tsuda, Takashi Taniguchi**



**Materials emitting light in the deep ultraviolet region around 200 nanometers are essential in a wide-range of applications, such as information storage technology, environmental protection, and medical treatment. Hexagonal boron nitride (hBN), which was recently found to be a promising deep ultraviolet light emitter, has traditionally been synthesized under high pressure and at high temperature. We successfully synthesized high-purity hBN crystals at atmospheric pressure by using a nickel-molybdenum solvent. The obtained hBN crystals emitted intense 215-nanometer luminescence at room temperature. This study demonstrates an easier way to grow high-quality hBN crystals, through their liquid-phase deposition on a substrate at atmospheric pressure.**


Hexagonal boron nitride (hBN) and cubic boron nitride (cBN) are known as the representative crystal structures of BN. hBN is chemically and thermally stable and has been widely used as an electrical insulator and heat-resistant material for several decades; cBN, which is a high-density phase, is almost as hard as diamond (*1*).

Promising semiconductor characteristics due to a direct band gap of 5.97 eV were recently discovered in high-purity hBN crystals obtained by a high-pressure flux method, paving the way for a material that efficiently emits deep ultraviolet (DUV) light (*2*, *3*). Similar to aluminum nitride (AlN) (*4*) and gallium nitride (GaN) (*5*), hBN may have attractive potential as a wide–band gap material. The layered structure of hBN makes the material mechanically weak, but it has greater chemical and thermal stability than GaN and AlN. The interesting optical properties of hBN, such as its huge exciton-binding energy (*2*), are due to its anisotropic structure, whereas a single crystal's basal plane in hBN is not easily broken because of its strong in-plane bonds. Thus far, the excitation of hBN by an accelerated electron beam or by far-UV light above the band-gap energy shows various efficient luminescence bands near the band edge.

However, the electronic properties of hBN near the band gap, which is fundamental information for developing DUV light–emission applications, are not yet fully understood, as seen by the fact that the origins of the luminescence bands are still controversial (*2*, *6*, *7*). Two opposed models, a Wannier exciton model and a Frenkel exciton model, have been proposed. The former model is based on results of the intrinsic absorption spectra near the band edge from pure single crystals (*2*), and the latter model is based on theoretical calculations and a luminescence study that used powder samples (*7*) showing very intense impurity bands around 4.0 eV (*8*). According to work examining the correlation between impurities and defects and luminescence properties (*8*, *9*), the intrinsic optical properties of samples are hindered by the extrinsic ones if experimenters do not have careful control of the samples' crystallinity and polymorphic purity. In (*7*), the strong 5.46-eV luminescence band, which is attributed to stacking faults (*9*), dominated in the region of the band gap, and the most intense photoluminescence band at 215 nm, observed in a pure single crystal, was not observed from the powder sample. Pure samples with high crystallinity must be indispensable for developing this new material for DUV light–emitting applications. Because high-quality hBN crystals have so far been produced only by high-pressure processes, it is important to discover an alternative synthesis scheme for conventional crystal growth at atmospheric pressure.

DUV-luminous single-crystalline hBN has been created through the reduction of O and C impurities with the use of a reactive solvent of the Ba-BN system under high pressure (*2*, *3*, *8*).


National Institute for Materials Science (NIMS), Tsukuba, Ibaraki 305-0044, Japan.

*To whom correspondence should be addressed. E-mail: kubota.yoichi@nims.go.jp